The Aeronautical Journal (2025), **129**, pp. 2283–2306
doi:10.1017/aer.2025.14

RESEARCH ARTICLE

Performance modelling and numerical simulation validation of hypersonic inlet with fuel pre-injection

F.T. Luo , H.T. Li , Z.M. Qu , W.J. Chen and Y.S. Long

School of Aerospace Engineering, Huazhong University of Science and Technology, Wuhan, 430074, P.R. China
Corresponding author: W.J. Chen; Email: chenwenjuan@hust.edu.cn

Received: 11 November 2024; **Revised:** 6 January 2025; **Accepted:** 11 February 2025

Keywords: inlet pre-injection; model analysis; injection model; numerical simulation; performance parameter

Abstract

Fuel pre-injection in the inlet of a hypersonic engine has been proven to be advantageous in the range of the very high flight Mach numbers. In this paper, a rapid inlet performance analysis model with fuel pre-injection is proposed. The modelling process is divided into two stages. Firstly, the baseline inlet model is provided based on the working principle of the inlet. Then, the newly proposed fuel injection and heat release model is added to the baseline inlet model. Among them, the fuel injection and heat release model is equivalent to increasing the compression angle in the cold state. And in the hot state the effect of the fuel heat release will be considered in addition to the effect of cold state. The research results show as the equivalence ratio increases, the equivalent compression angle also increases, but the two are not in a linear relationship. Based on this pattern of effect, fuel injection can be used to regulate the shock wave position and accurately control the flow rate of the inlet. In addition, by comparing to numerical simulation, it is found that the analysis model can almost reasonably predict the performance of the pre-injection inlet. However, the calculation of drag coefficient has some deviation compared to numerical simulation, which is probably due to the lack of consideration of friction drag and the interaction between the shock wave and boundary layer in the model analysis. Overall, the modelling method proposed in this paper can reflect the effect of fuel injection on inlet performance, which can be used to optimise injection strategy in the future.

Nomenclature

A	area (m^2)
C	drag coefficient
h	fuel penetration depth (m)
H	total enthalpy (kJ/kg)
m	mass flow rate (kg/s)
M	Mach number
P	static pressure (Pa)
P_t	total pressure (Pa)
T	static temperature (k)
V	velocity (m/s)
AUSM	advection upstream splitting method
CR	contraction ratio
DPM	discrete phase model
ER	equivalence ratio
RBCC	rocket-based combined cycle engine

Greek Symbol

α	fuel injection angle (deg)
β	oblique shock angle (deg)

© The Author(s), 2025. Published by Cambridge University Press on behalf of Royal Aeronautical Society.

https://doi.org/10.1017/aer.2025.14 Published online by Cambridge University Press

γ	specific heat ratio
δ	deflection angle (deg)
φ	flow coefficient
ρ	density (kg/m^3)
θ	cowl angle (deg)
σ	total pressure recovery coefficient
μ	boundary layer thickness

Subscripts

0	free stream conditions
f	fuel

1.0 Introduction

Hypersonic vehicle has become the main strategic direction of future aircraft, whose flying height can be 0 ∼ 30km or higher, and power device is the key to the realisation of hypersonic flight. At present, a scramjet engine can be regarded as the most suitable propulsion system for air-breathing hypersonic vehicle [1–4]. Though the high specific impulse and simple structure make the scramjet concept appealing at high Mach numbers, the combustion aspect of the engine faces challenges related to ignition and sustaining combustion in high-speed gas flows. These challenges arise from factors such as reduced residence time and poor mixing efficiency within the combustion chamber due to the supersonic airflow [5]. To improve the engine performance, researchers have focused on how to promote the combustion efficiency, such as adjusting fuel injection schemes, enhancing flame stabilisation, and improving supersonic ignition and combustion [6–9]. But these technologies occurred in the combustion chamber.

As research progresses, it has been discovered that pre-injection of fuel in hypersonic inlets can decrease the combustion chamber mixing length of the fuel by fuel mixing in advance and may also be utilised for inlet shock and flow control, which has been illustrated to be indeed practical [10–15]. Guoskov et al. [10] conducted experiments demonstrating that enhanced fuel mixing efficiency can be achieved by the pre-injection of a mixture of ethylene and propane. And a rationale for the choice of the pylon/fuel injector positions is suggested that can provide mixing efficiency levels up to 0.95∼0.98 at the inlet exit using fuel rates corresponding to fuel/air equivalence ratios of 0.25∼0.66. Furthermore, Kim et al. [11] chose an orifice injector instead of cantilevered injectors to investigate the effects of pre-injection in the inlet on mixing efficiency. The research results showed that by varying the injection angle, ER, and compression ramp angle, the reflection of shock waves on the inner wall of the inlet significantly influenced the mixture efficiency. The main challenge of injecting hydrogen fuel through the inlet is preventing premature ignition of the hydrogen fuel. Zhu et al. [12] conducted numerical simulation focusing on fuel control of shock waves and self-mixing of the fuel. By adjusting the fuel injection pressure of the five injection nozzles, they found that a hypersonic inlet designed for Mach 5 could still achieve shockwave intersection at the cowl lip for the design point of Mach 6. However, the practicality of inlet pre-injection also presents certain challenges. Gardner et al. [13] tried to check whether pre-combustion would appear in the inlet. The experimental results indicated that no pre-combustion existed in hypersonic inlet even for the wall temperature of 700K. Similarly, Turner and Smart [14,15] found the corresponding conclusions by conducting experimental studies on hydrogen fuel injection through the inlet under conditions where the inflow was Mach 8. The results demonstrated that fuel injection in the inlet did not lead to pre-combustion, allowing for greater pressure rise but also increasing the drag. However, for equivalence ratio (ER) exceeding 0.92, inlet pre-injection may make the inlet unstart.

To sum up, the implementation of fuel pre-injection in the inlet has achieved fuel premixing and enhanced fuel mixture efficiency, but it has also brought certain negative effects, such as increased drag [16–18]. In extreme cases, it may also cause the inlet not to start. The main reason for the above negative

https://doi.org/10.1017/aer.2025.14 Published online by Cambridge University Press

effects is fuel injection may alter the original wave configuration of the inlet and lead to a reduction in flow rate. Fuel injection not only affects mixing efficiency, but also impacts the performance of the inlet, which requires the performance analysis of inlet with pre-injection not to be limited to the inlet itself, but rather should extend to the entire engine. Using numerical simulation to analyse the performance of the entire engine will consume a lot of time and is not conducive to optimisation of the performance of the inlet. Within the acceptable range of computational accuracy, the simplified mathematical models with a small amount of computation to perform preliminary performance analysis is a more reasonable choice. Dalle et al. [19] proposed an analytical model to predict a steady two-dimensional supersonic flow through an inlet. The results were compared to experimental data, and the model inaccuracies were found to be limited to 10%. Additionally, Dalle et al. [20] also adopted to an analytical model to improve inlet performance by using a variable-geometry cowl. Investigating flight at a range of conditions shows that variable geometry can strongly improve inlet performance. Zhang et al. [21] established a rocket-based combined cycle engine (RBCC) model with high accuracy and adaptability, including the ejection-mode model, dual-mode scramjet model and rocket-mode model. And taking a typical RBCC launch vehicle as an example, the wide-speed performance of the RBCC propulsion system is calculated and analysed.

Based on the current research status, it can be seen that the analytical model has been widely used in the performance evaluation of inlet and scramjet engines. However, few scholars have conducted performance analysis of pre-injection inlets based on the analytical model, mainly due to the limitations of immature fuel pre-injection model of inlet. Faced with the problem of immature pre-injection model, this paper proposes a simplified fuel pre-injection model based on the working process of fuel injection and conduct performance modelling for inlets with pre-injection. In addition, the numerical simulation of pre-injection inlet is also done to verify the correctness of the modelling method. In the future, the modelling method proposed in this paper is able to provide assistance for optimising injection strategies and improving the scramjet engine performance. This paper is structured as follows. Section 2 mainly provides a design methodology of hypersonic inlet with pre-injection and a detailed process to the performance modelling of inlet with fuel pre-injection. Section 3 presents inlet geometry model and numerical method. Section 4 presents the results and discussion of the hypersonic inlet with pre-injection, including design and analysis of the geometric parameter, effect of fuel injection and heat release and comparative analysis of modelling and numerical simulation. Finally, section 5 presents the main conclusions obtained from the configurations analysed.

2.0 Description of methodology and models

2.1 Design methodology of hypersonic inlet with pre-injection

Figure 1 shows the geometry and shock wave configurations of traditional scramjet and scramjet with pre-injection inlet. It is evident that the scramjet with pre-injection inlet has a relatively shorter size. This is because the inlet design Mach number of two scramjets is different. The traditional inlet is designed based on a high Mach number as the design point to avoid over-rating. However, it is inevitable that the flow coefficient is low when the inflow is at a low Mach number. On the contrary, the pre-injection inlet is designed with a low Mach number as a design point, and the shock wave configurations is adjusted through fuel injection during high Mach number inflow, which can also prevent the inlet from entering an over-rated state. Since it is designed at the low Mach number, the overall flow coefficient is relatively high. Additionally, due to early fuel injection, the fuel mixing distance is extended.

The basic configuration of the pre-injection inlet designed in this paper is shown in Fig. 2, which uses a two-dimensional mixed-compression structure with three external compression shock waves and two internal compression shock waves. The geometric design process for pre-injection inlets can be divided into two parts: one is the geometric design of inner surface, and the other is the pre-injection parameters. Figure 3 shows the simplified design process. The geometric design of the inner surface can be determined by the theory of equal shock wave intensity [22]. By providing a deflection angle and contraction ratio, a certain inlet geometry can be obtained through the iterative calculations.

https://doi.org/10.1017/aer.2025.14 Published online by Cambridge University Press

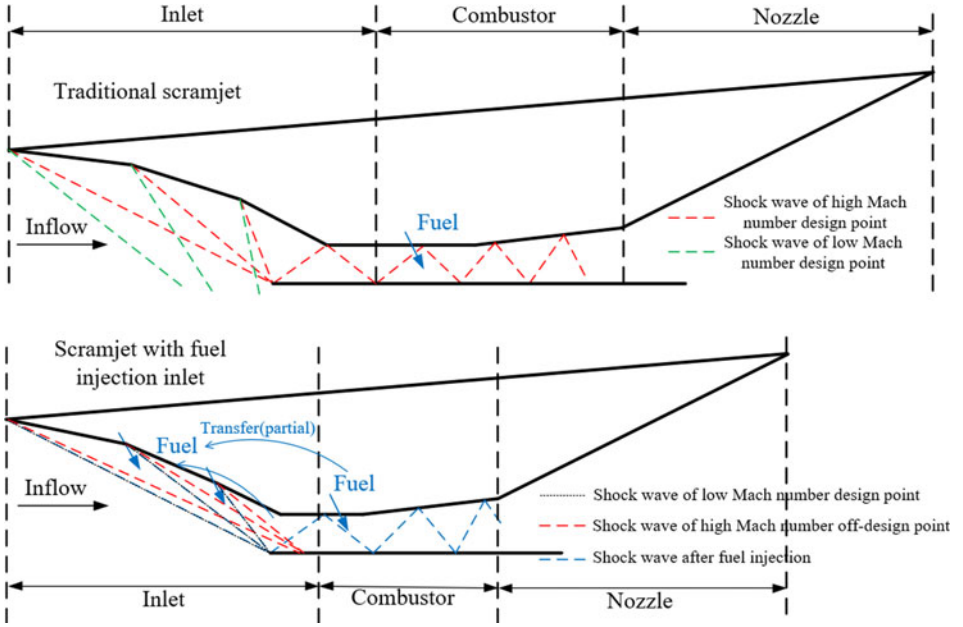


Figure 1. *The geometry and shock wave configurations of traditional scramjet and scramjet with pre-injection.*

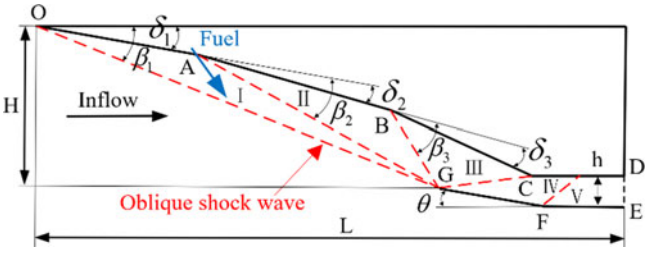


Figure 2. *Schematic diagram of inlet.*

Taking a two-dimensional inlet as an example in Fig. 2, the design process of specific equal shock intensity is shown as follows. The initial value of the first deflection angle δ_1 is given, and the first oblique shock angle β_1 and corresponding gas parameters in zone I are obtained by using the oblique shock model. Based on the equal shock intensity Equation (1), the second oblique shock angle β_2 and corresponding gas parameters in zone II can be calculated. Similarly, the third oblique shock angle β_3 and corresponding gas parameters in zone III can also be obtained.

$$M_0 \sin \beta_1 = M_1 \sin \beta_2 = M_2 \sin \beta_3 \tag{1}$$

And the second and third deflection angles δ_2 and δ_3 can be determined based on the second and third oblique shock angles and parameters before and after the oblique shock wave. With the given total deflection angle δ_2, the first deflection angle δ_1 of the next iteration is updated. The above calculations are repeated iteratively to update the three deflection angles δ_1, δ_2 and δ_3 until the desired accuracy ε is satisfied.

$$|\delta - (\delta_1 + \delta_2 + \delta_3)| \leq \varepsilon \tag{2}$$

https://doi.org/10.1017/aer.2025.14 Published online by Cambridge University Press

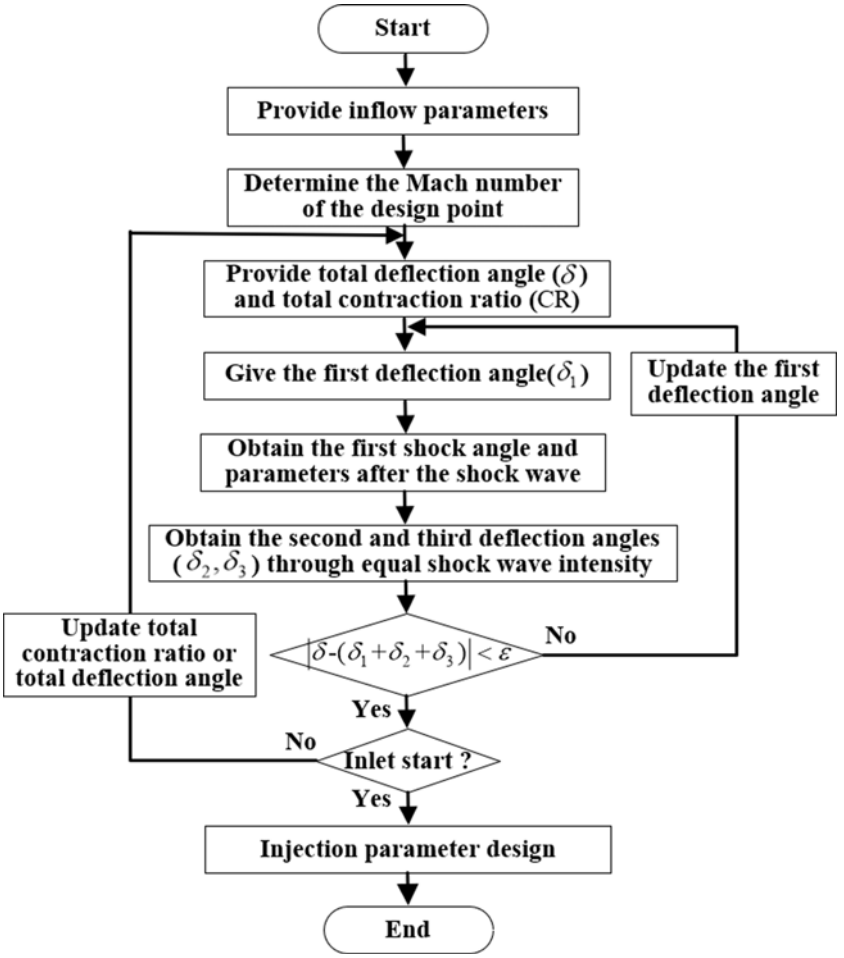


Figure 3. *Design process of inlet with fuel pre-injection.*

After determining the three deflection angles δ_1, δ_2 and δ_3, the fourth deflection angle δ_4 and the fifth deflection angle δ_5 can be obtained based on the given total deflection angle δ using geometric relationships shown in Equation (3).

$$\begin{cases} \delta=\delta_1+\delta_2+\delta_3 \\ \delta_4=\delta-\theta \\ \delta_5=\theta \end{cases} \tag{3}$$

The calculation method for the fourth shock wave and the fifth shock wave are consistent with the previous oblique shock wave calculation. So far, all compression ramp angles, shock wave angles, as well as downstream parameters of the oblique shock wave have been determined.

Next, it is the selection of pre-injection parameters. The injection parameters mainly include the injection positions and injection angles. The selection of injection parameters should be based on overall performance, considering both the performance of the inlet itself and the effect on combustion performance, which requires a comprehensive balance. Without going into details here, the injection angle designed in this paper is perpendicular to the horizontal direction, and the injection location is starting position of the second compression ramp.

https://doi.org/10.1017/aer.2025.14 Published online by Cambridge University Press

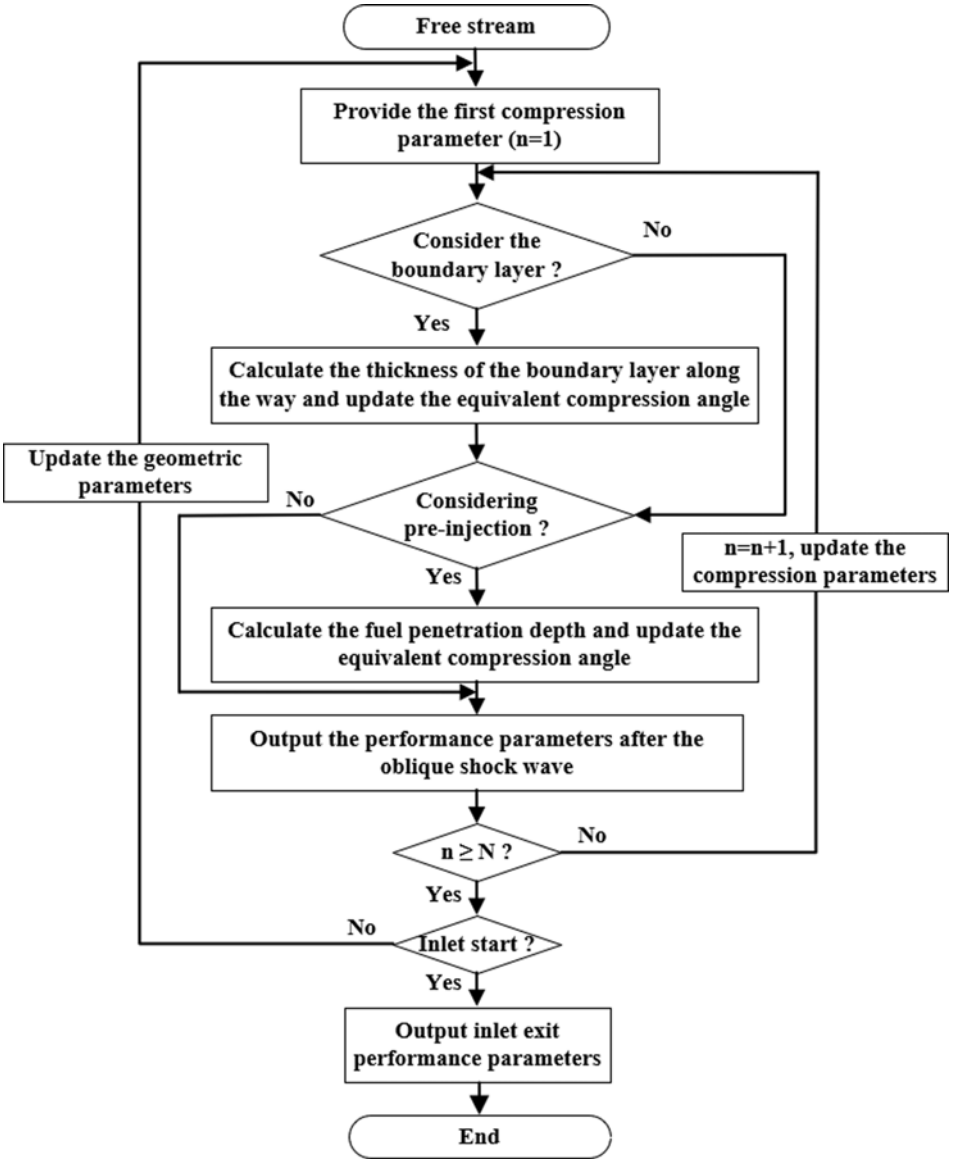


Figure 4. *Performance analysis process of inlet with pre-injection.*

2.2 Performance modelling of inlet with fuel pre-injection

A traditional two-dimensional inlet consists of multiple compression ramps and a cowl, so the modelling of the flow process mainly focuses on the calculation of the multiple shock compression process. Due to the presence of viscosity, the effect of boundary layer also needs to be considered. In addition, in order to determine whether the inlet is stable, the start of the inlet during the modelling process should also be kept continuous attention. However, when fuel injection is introduced, the injected fuel will hinder the inflow and may also react with the inflow. In order to simplify the complexity of modelling, a simplified pre-injection model is proposed to analyse the effect of fuel injection on the flow process. And the performance analysis process for a pre-injection inlet is given in Fig. 4. Among them, N represents the total number of the equal compression ramp and n represents the *nth* equal compression ramp.

https://doi.org/10.1017/aer.2025.14 Published online by Cambridge University Press

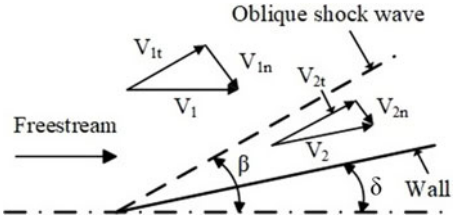


Figure 5. *Schematic diagram of oblique shock wave.*

2.2.1 Baseline inlet model

The traditional inlet is defined as the baseline inlet, which is an inlet without fuel pre-injection. And the key models involved in the modelling process of the baseline inlet will be described. The first is the oblique shock wave model, as shown in Fig. 5. Because the inflow is supersonic, the calculation of oblique shock wave needs to consider the variation of the specific heat ratio γ [23]. And the calculation process of oblique shock wave is given as follow. According to the compression characteristics of the oblique shock wave, the tangential velocity component along the shock wave remains unchanged.

$$V_{1t} = V_{2t} \tag{4}$$

The normal velocity component along the shock wave satisfies the following relation.

$$\frac{V_{2n}}{V_{1n}} = \frac{\tan(\beta - \delta)}{\tan\beta} \tag{5}$$

At the same time, the parameters before and after the shock wave satisfy the state Equation (6), flow conservation Equation (7), momentum conservation Equation (8) and energy conservation Equation (9).

$$P = \rho RT \tag{6}$$

$$\rho_1 V_{1n} = \rho_2 V_{2n} \tag{7}$$

$$P_1 - P_2 = \rho_2 V_{2n}^2 - \rho_1 V_{1n}^2 \tag{8}$$

$$H_1 + \frac{V_{1n}^2}{2} = H_2 + \frac{V_{2n}^2}{2} \tag{9}$$

Assuming that x and y are expressed as follows.

$$\begin{cases} x = \gamma_1 Ma_{1n}^2 \\ y = \gamma_2 Ma_{2n}^2 \end{cases} \tag{10}$$

where γ_1 and γ_2 are the specific heat ratios before and after the shock wave, which are not equal after considering the variable γ. Ma_{1n} and Ma_{2n} are the normal Mach numbers before and after the shock wave. From the flow conservation Equation (7) and momentum conservation Equation (8), the following relationship can be obtained by using the ideal gas state Equation (6) and the sonic equation.

$$y = \frac{1}{\left(\frac{1+x}{x}\right)\frac{\rho_2}{\rho_1} - 1} \tag{11}$$

The expressions for the pressure rise ratio, temperature rise ratio and conservation of energy equation before and after the shock wave can be further derived as follows.

$$\frac{P_2}{P_1} = \frac{1+x}{1+y} \tag{12}$$

https://doi.org/10.1017/aer.2025.14 Published online by Cambridge University Press

$$\frac{T_2}{T_1} = \frac{P_2}{P_1}\frac{\rho_1}{\rho_2} \tag{13}$$

$$H(T_1) + \frac{xRT_1}{2} = H(T_2) + \frac{yRT_2}{2} \tag{14}$$

By using the calculated downstream parameters of the first oblique shock wave as a known condition for the next oblique shock, and so on, it is possible to determine the downstream parameters for multiple oblique shock waves.

Next, the effect of the boundary layer is considered. In the inlet configuration of this paper, the leading edge of inlet is taken as the starting point for the development of boundary layer, and the boundary layer gradually grows along the compression ramp. After calculating the thickness of boundary layer, it is assumed that the sum of the original ramp height and the corresponding boundary layer thickness is the equivalent compression ramp height. And the external compression ramp angle of the inlet is updated, and then each shock wave angle is updated to obtain the flow parameters in each region. Among them, the boundary layer thickness calculation is based on the conclusions of reference [24], and the calculation Equation (15) is provided when the Reynolds number, *Re*, is at the order of 10^6.

$$\begin{cases} \mu_1 = 0.37X\ \mathrm{Re}^{-1/5} \\ \mu_2 = 0.036\left(1 + M^2/10\right)^{-0.70} X\ \mathrm{Re}^{-1/5} \\ \mu_3 = 0.046\left(1 + 0.8M^2\right)^{0.44} X\ \mathrm{Re}^{-1/5} \end{cases} \tag{15}$$

When the Reynolds number, *Re*, reaches the magnitude of 10^7, the following calculation Equation (16) is presented.

$$\begin{cases} \mu_1 = 0.23X\ \mathrm{Re}^{-1/6} \\ \mu_2 = 0.022\left(1 + M^2/10\right)^{-0.70} X\ \mathrm{Re}^{-1/6} \\ \mu_3 = 0.028\left(1 + 0.8M^2\right)^{0.44} X\ \mathrm{Re}^{-1/6} \end{cases} \tag{16}$$

Among them,

$$\begin{cases} X = P^{-1}\int_0^x P dx \\ P = \left[M/\left(1 + M^2/5\right)\right]^4 \end{cases} \tag{17}$$

In the Equation (15) and (16), M represents the Mach number of free stream, x denotes the distance along the flow direction, μ_1 is the velocity boundary layer thickness, μ_2 is the momentum loss thickness, and μ_3 is the displacement thickness.

At last, due to the particularity of the inlet, the starting ability of the inlet should be taken into consideration. Moreover, different types of inlets have different methods of starting identification. The starting process of a mixed compression inlet is similar to that of an internal compression inlet, but there are also differences that require a thorough consideration of the effect of external compression shock waves, as well as a meticulous study of the effect of boundary layer. These factors make the starting problem of a mixed compression inlet relatively complex. The starting judgment formula of the inlet in this paper adopts the following empirical formula [25].

$$\frac{A_0}{A_t} = \frac{1}{0.05 - 0.52/Ma_0 + 3.56/Ma_0^2} \tag{18}$$

where A_0 is the capture area of inlet entrance, A_t is the inlet throat area and Ma_0 is the inflow Mach number.

2.2.1 Fuel pre-injection and heat release model

The effect of fuel injection on the performance of inlet can be divided into cold state and hot state. In the cold state, there is no reaction and fuel injection only affect the flow state. Shock waves, including

https://doi.org/10.1017/aer.2025.14 Published online by Cambridge University Press

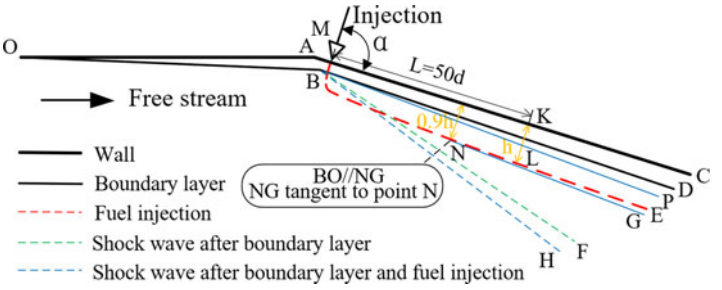


Figure 6. *Equivalent model of fuel pre-injection.*

bow shock and barrel shock, will be induced after fuel injection, which can be coupled with the initial oblique shock wave of the inlet. Therefore, such a complex coupling process is difficult to be directly described by mathematical models. Here, this paper makes the following assumptions. First, the structure of the boundary layer at the injection position will be destroyed, affecting the original shock wave. The fuel injection will also induce new shock waves. In this paper, the effects of fuel injection on the flow field are transformed into the effect on equivalent compression ramp [26]. Secondly, considering that the frictional force gradually changes along the wall, flow parameters need to be calculated based on microelements, which requires a lot of time. Moreover, the effect of wall friction on flow parameters is also small [19, 27], and the focus of this paper is to study the characteristics of inlet fuel injection modelling. Therefore, the effect of wall friction is ignored in the modelling process.

Based on the above assumptions, the model for fuel pre-injection into the inlet can be shown in Fig. 6. First, calculate the penetration depth of fuel based on the injection state. Because the penetration depth increases gradually along the flow direction, and the increase rate of penetration depth decreases gradually as the flow distance increases. In the paper, the penetration depth h corresponding to a distance of 50 times the diameter of the injection hole is taken as the final penetration depth. Then, make a tangent NG at a depth of 0.9 times penetration depth ($0.9h$) and obtain a slope k of the tangent NG, and use the straight line BP with the slope k passing through point B as the equivalent ramp to consider the effect of fuel pre-injection. Finally, based on the equivalent compression ramp BP, a new shock wave BH instead of the original shock wave BF is obtained.

Among them, the formula for calculating the fuel penetration depth [28] is shown in Equation (19). In this equation, h represents the fuel penetration depth, D indicates the axial characteristic diameter of the fuel injector, q_j and $q_{a,}$ respectively, represents the momentum of the fuel jet and incoming flow, x stands for the fuel diffusion distance, α denotes the fuel injection angle and AR represents the ratio between the equivalent diameter of the fuel injector and its transverse characteristic diameter.

$$\frac{h}{D} = const\left(\frac{q_j}{q_a}\right)^{0.5} (AR)^{0.46} \ln\left[1 + 6\frac{x}{D}\right] \sin\left(\frac{2\alpha}{3}\right) \tag{19}$$

While in the hot state, there is a fuel reaction and heat release. After obtaining the effect of cold-state injection on the flow field, the calculations for the fuel mixing and combustion heat release are performed. And the analysis of fuel heat release is mainly based on fuel mixture, which requires obtaining the mixture efficiency of fuel along the flow direction. The mixture efficiency of hydrogen fuel is determined by using the empirical Equation (20) from reference [29].

$$\eta_m = a\left(1 - e^{(-(k\bar{x})^d)}\right) \tag{20}$$

Among them, a, k and d are constants with values $a = 1.06492$, $k = 3.69639$, $d = 0.80586$. The normalised distance along the ramp is defined as $\bar{x} = x/L_{mix}$. The mixing length can be calculated using

https://doi.org/10.1017/aer.2025.14 Published online by Cambridge University Press

the following Equation (21).

$$\frac{L_{mix}}{d_F} = \frac{K^*}{f(M_c)}\left(\frac{\rho_f U_f}{\rho U}\right)^{\frac{1}{2}} \tag{21}$$

where d_F is the injector hydraulic diameter, the character f indicates fuel properties and $K*$ is a constant that depends on the type of injection system and a variety of other injection flow field interaction parameters. The constant $K*$ is found by using the multi-dimensional CFD results of reference [30]. In their work, mixing efficiency was calculated along a hydrogen-fuelled strut injected scramjet duct and compared with experimental measurements. Using the results from the above study, the value of the constant was found to be $K* = 390$. And the functions $f(M_c)$ is given as follows.

$$f(M_c) = 0.25 + 0.75e^{-3M_c^2} \tag{22}$$

where M_c is defined in Equation (23).

$$M_c = \frac{U_f - U_a}{a_f + a_a} \tag{23}$$

In the equation, U_f is the fuel injection speed, U_a is the velocity of incoming air, a_f and a_a are the local sound speed fuel and air. The calculation of mixing efficiency is carried out under the given inflow and injection conditions. After obtaining the mixing efficiency, it is assumed that the combustion efficiency is equal to the mixing efficiency, and the total temperature of the combustion products are calculated. Based on energy conservation, the total enthalpy and total temperature of the mixture shown in Equation (24) are obtained by using the total temperature of air and combustion products, and the static temperature T_{mix} of the mixture will be obtained. Among them, I represents the different type of gas.

$$\begin{cases} H(T_{tmix}) = \sum H_i(T_{ti}) \\ H(T_{tmix}) = H(T_{mix}) + \frac{V^2}{2} \end{cases} \tag{24}$$

Subsequently, the specific heat ratio, gas constant and other state parameters of mixture can be also obtained by using the different component concentration.

2.3 Definition of inlet performance parameters

To meet the needs of research and analysis, relevant performance parameters should be defined. The flow coefficient ϕ is used to evaluate the amount of freestream entering the inlet [31]. It is defined as

$$\varphi = \frac{m}{m_0} \tag{25}$$

where m is the actual mass flow rate into the inlet, m_0 is the mass flow rate through the capture area in the freestream state. And throat Mach number is defined as the Mach number at the throat.

The total pressure recovery coefficient σ is used to evaluate the loss of total pressure due to shock waves and viscosity [31]. It is defined as

$$\sigma = \frac{p_t}{p_{t0}} \tag{26}$$

where p_t is mean total pressure at the inlet exit, p_{t0} is freestream total pressure. The definition of drag coefficient is shown as follows [31].

$$C = \frac{F}{\frac{1}{2}\rho_0 V_0^2 A_{in}} \tag{27}$$

where F is the drag; ρ_0 is the density of freestream; V_0 is the velocity of freestream; A_m is the capture area of freestream. The static pressure ratio is defined as the ratio of static pressure at the inlet exit to

https://doi.org/10.1017/aer.2025.14 Published online by Cambridge University Press

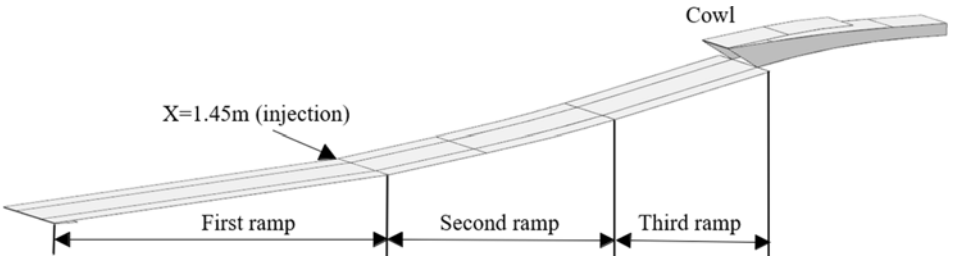


Figure 7. *The geometric model of inlet.*

static pressure of freestream [31]. This expression is shown in Equation (28).

$$\psi_p = \frac{p}{p_0} \tag{28}$$

where p is mean static pressure at the inlet exit, p_0 is static pressure of freestream. Similarly, the static temperature ratio is defined as the ratio of temperature pressure at the inlet exit to static temperature of freestream [31]. This expression is shown in Equation (29).

$$\psi_T = \frac{T}{T_0} \tag{29}$$

where T is mean static temperature at the inlet exit, T_0 is static temperature of freestream.

3.0 Numerical simulation method and validation

3.1 Geometric model

As shown in Fig. 7, the geometric model of the inlet adopts a two-dimensional mixed compression structure from the model design, and the external compression section is the three-stage compression. The total length of the inlet is 3.9 m with the contraction ratio 10 and deflection angle 12.8°, and the cowl angle is 8°. The fuel pre-injection position is set at $X = 1.45$m and injection holes are perpendicular to the second ramp. There are 10 injection holes and the interval between the injection holes is 5mm [32]. The injection parameters are controlled by discrete phase model (DPM), and the injection flow rate changes with the change of fuel equivalence ratio. In the DPM, injection type is cone and outer radius of injection hole is 0.00035m. In order to reduce the total pressure loss of the inlet, smoothing treatment is applied at the shoulder and cowl lip. Five bleed slots are arranged at the shoulder position of the compression ramp to remove the boundary layer flow. Based on the design of the shock wave configuration, a 3mm radius passivation was performed on the leading edge of the first ramp and cowl lip to simulate the actual passivation effect.

3.2 Numerical method and meshes

The numerical simulation is performed by using a commercial solver Fluent. And the calculation method is based on the steady Reynolds-averaged N-S equations with the finite volume method and the shear stress transport k-ω turbulence model. Its accuracy has been validated in many references [33–35]. To provide exact resolution of shock discontinuities, the advection upstream splitting method (AUSM) is employed for the approximation of the convective flux splitting and the governing equations are discretised by the second-order upwind method. The density-based solver with second-order spatial accuracy is used for the implicit solution. In addition, during the simulation of the injection process the DPM is used to model the hydrogen fuel injection. Among them, the main components of the combustion reaction include O_2, H_2, H_2O, O, H, OH, HO_2, H_2O_2, N_2, and the laminar finite rate model is selected for calculation [36].

https://doi.org/10.1017/aer.2025.14 Published online by Cambridge University Press

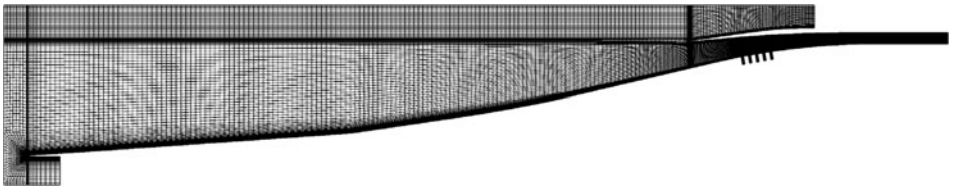


Figure 8. *Schematic diagram of scramjet mesh.*

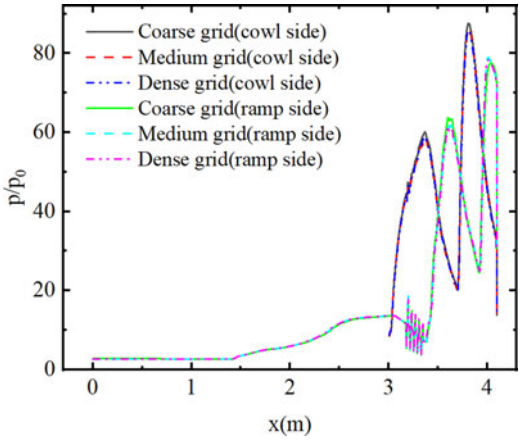


Figure 9. *Comparison of static wall pressure.*

Considering that the two-dimensional configuration of the inlet is symmetrical, only half of the flow region can be taken into account for computation. The software ICEM is used to generate the grid, and a hexahedral structured grid will be used. The grid diagram is shown in Fig. 8. It can be seen that the near-wall regions have been refined based on a y^+ value below 1. The far field of the inlet adopts pressure far field, and the wall boundary conditions are both adiabatic and non-slip wall conditions. Meanwhile, in order to verify grid independence, a simulation of the above inlet with a coarse grid (80,000), medium grid (150,000) and dense grid (250,000) was done, and the freestream Mach number, total temperature and static pressure were 10, 4117.9 K and 571.59Pa, respectively. Figure 9 shows the comparison of static wall pressure (p is the static pressure and subscript "0" denotes the freestream parameter) under different grid scales. It can be seen that there are high frequency fluctuations in ramp side because of the effect of bleed slots. And it is easy to know that the medium and dense grid show the same trend, and the coarse grid has a slight deviation. So the medium and dense grid represents more adequately the flow behaviour. Taking into account the calculation cost and simulation accuracy requirements, the medium grid with 150,000 cells is finally chosen for subsequent simulations.

3.3 Numerical method validation

To thoroughly validate the accuracy of numerical simulation method, a three-dimensional simulation is performed and the geometry model is the same as the experimental engine of Odam [37]. The experimental engine has a total length of 625mm, width of 75mm and a combustion chamber height that can be adjusted between 20 and 30mm. In this study, a combustion chamber height of 24mm is used. For a detailed description of the geometric configuration, please refer to the reference [37]. Due to the axisymmetric distribution of the engine configuration, a quarter of the geometry model is taken into account for calculations. The corresponding structured grid is used, as shown in Fig. 10, and the total number of

https://doi.org/10.1017/aer.2025.14 Published online by Cambridge University Press

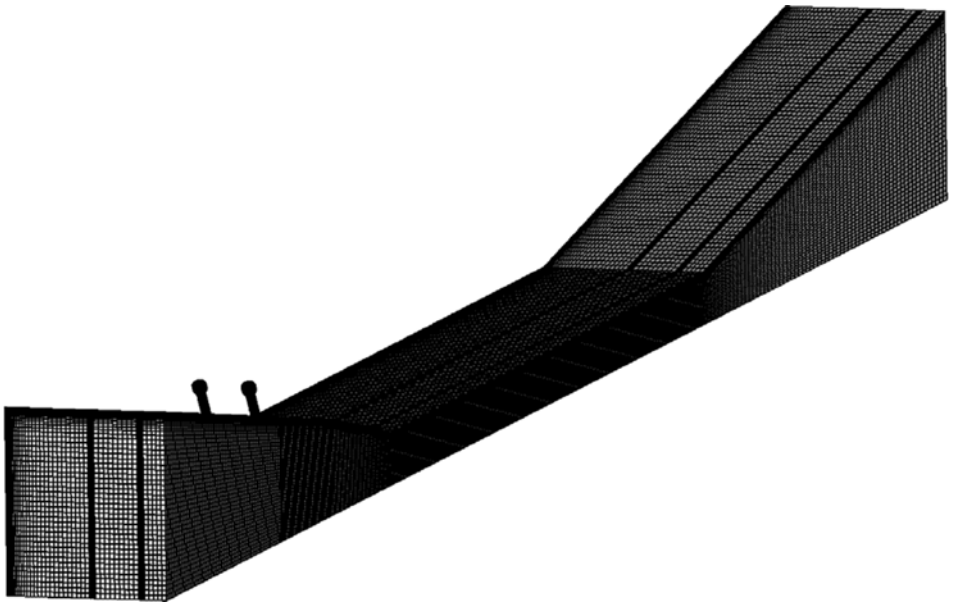


Figure 10. *Schematic diagram of Hyshot-II engine mesh.*

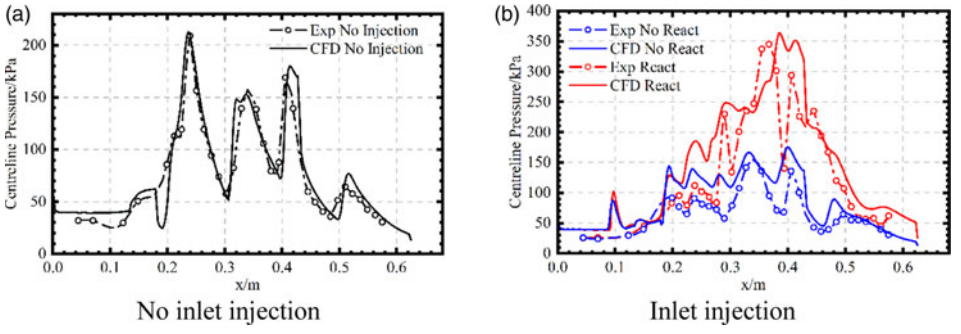


Figure 11. *Pressure distribution along the Hyshot-II engine wall.*

grids is 1.5 million. Figure 11 shows the comparison of numerical simulation and experimental results between no inlet pre-injection and inlet pre-injection. From the Fig. 11, it could be seen that the wall pressure distribution of the numerical simulation and experiment is basically consistent. But there are some deviations in the local position, which may be due to the non-uniform effect of inflow, the heat transfer effect, the three-dimensional effect, the deficiency of the turbulence model or the experimental measurement error. In addition, Figure 12 compares the numerical schlieren images with the experimental schlieren images under the combustion condition, showing similar oblique shock wave features. Overall, it can be concluded that the calculation method used in this study can reasonably simulate the flow process of the high Mach number in the scramjet engine.

4.0 Results and analysis

4.1 Design and analysis of the geometric parameter

Based on the design characteristic of the inlet with pre-injection and the operating range of Mach 7∼12, Mach 8.5 is selected as the design point. At design point Mach 8.5 the inlet performance curves are

https://doi.org/10.1017/aer.2025.14 Published online by Cambridge University Press

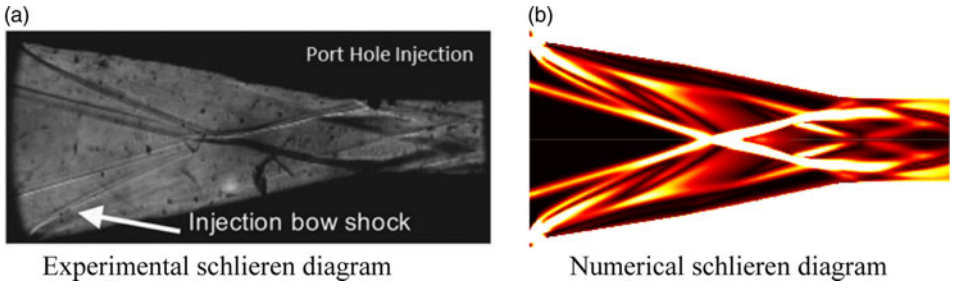


Figure 12. *Comparison of experimental and simulated schlieren images.*

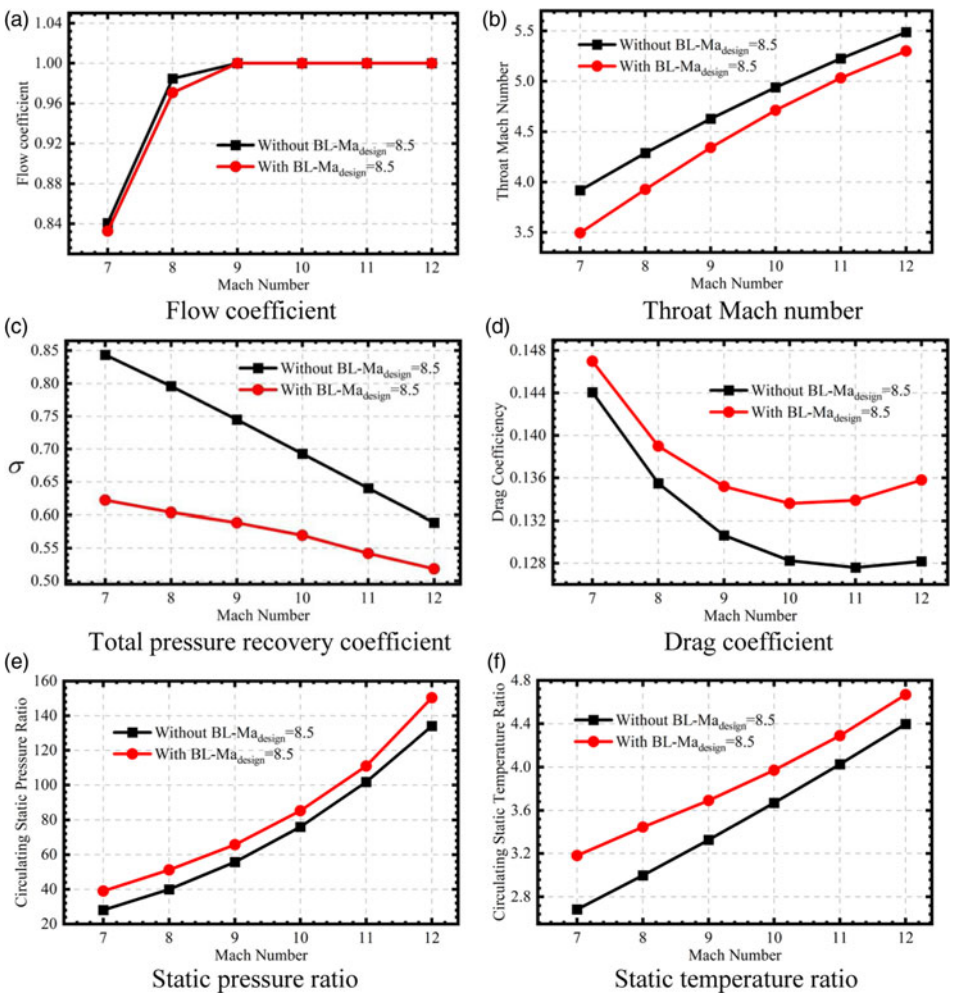


Figure 13. *Performance comparison with or without the boundary layer.*

shown in Fig. 13. As the inflow Mach number increases, the state of the inlet gradually approaches the design point, and the flow coefficient increases. However, when the Mach number exceeds Mach 8.5, the flow coefficient remains at its maximum value of 1, and the inlet enters the overrated state. The increase of inflow Mach number results in an increase in throat Mach number and total pressure loss. Under hypersonic flow conditions, the effect of boundary layer on the performance of the inlet cannot

https://doi.org/10.1017/aer.2025.14 Published online by Cambridge University Press

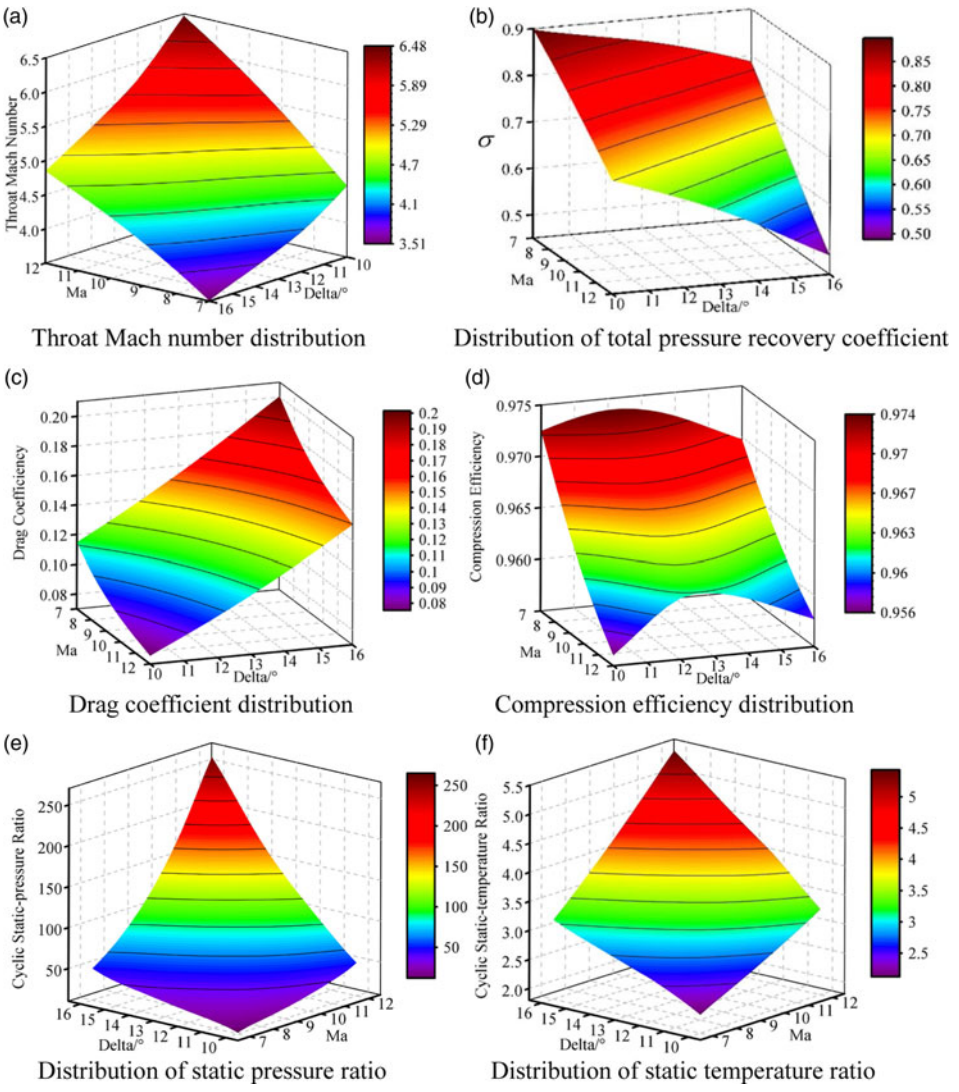


Figure 14. *Variation trend of inlet performance with total deviation angle.*

be ignored. The performance curve of the inlet, considering the boundary layer, shows a decrease in the flow coefficient at Mach 7 and 8, indicating that the presence of boundary layer leads to an increase in the external compression shock angle. Additionally, the presence of the boundary layer in the low-speed region results in lower throat Mach numbers compared to cases without the boundary layer, leading to relatively higher total pressure losses.

When designing the geometric parameter of the inlet, the total deflection angle and CR need to be designed with emphasis. The two factors mainly affect the performance parameters of the inlet. And the following analysis will focus on the two design parameters. Firstly, using the total deflection angle as a variable, the inlet performance parameters are obtained at the design point Mach number with total deflection angles of 10°, 12°, 12.8°, 14° and 16°, as shown in Fig. 14. Since all operating conditions are at the design point, the flow coefficients are all equal to 1. If the total deflection angle of the inlet is increased, the compression degree of the incoming flow gradually increases, and the Mach number at the throat decreases. The cyclic static pressure ratio and the cyclic static temperature ratio increase, but correspondingly, the total pressure loss and the drag coefficient also increase. In addition, as the design

https://doi.org/10.1017/aer.2025.14 Published online by Cambridge University Press

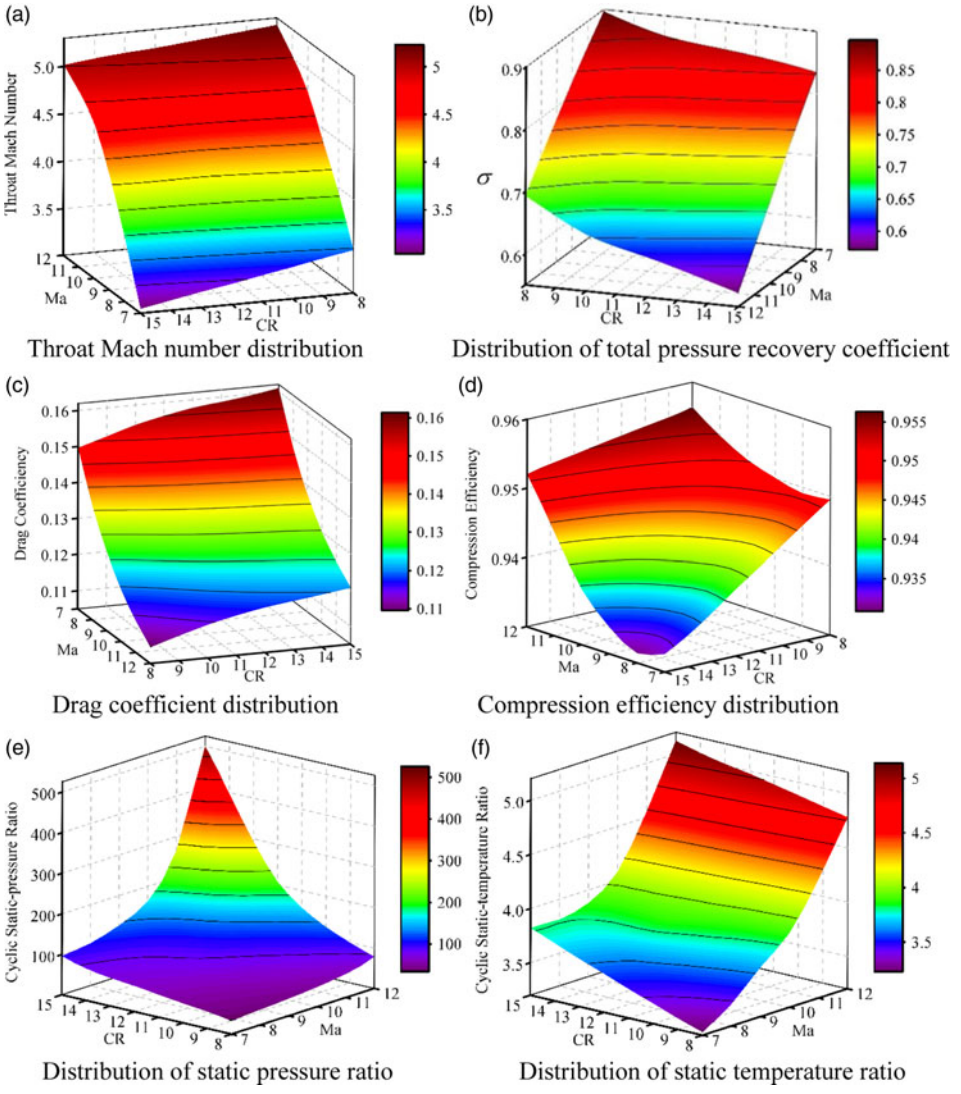


Figure 15. *Variation trend of inlet performance with total contraction ratio.*

Mach number increases, the cyclic static temperature ratio and cyclic static pressure ratio gradually increase, while the total pressure recovery coefficient and drag coefficient gradually decrease.

Secondly, taking the CR as a variable, the inlet performance parameters are obtained under different CR conditions, as shown in Fig. 15. Due to only changing the CR, deflection angle, shock wave angle and inflow parameters do not change, and only the height of the throat will change. However, after introducing the boundary layer factor, the proportion of boundary layer thickness will change under different throat heights, ultimately resulting in changes in inlet performance parameters with CR. Therefore, the performance graphs presented here are all based on considering the boundary layer factor. It is observed that increasing the CR of inlet gradually enhances the compression of the inflow. This leads to a decrease in the throat Mach number and total pressure recovery coefficient, while to some extent increasing the cyclic static pressure ratio and cyclic static temperature ratio. The increase of the CR also leads to the increase of the windward area of inlet, and the increase of the pressure drag, which makes the drag coefficient of inlet increase. Therefore, the overall compression efficiency of inlet decreases with the increase of the CR.

https://doi.org/10.1017/aer.2025.14 Published online by Cambridge University Press

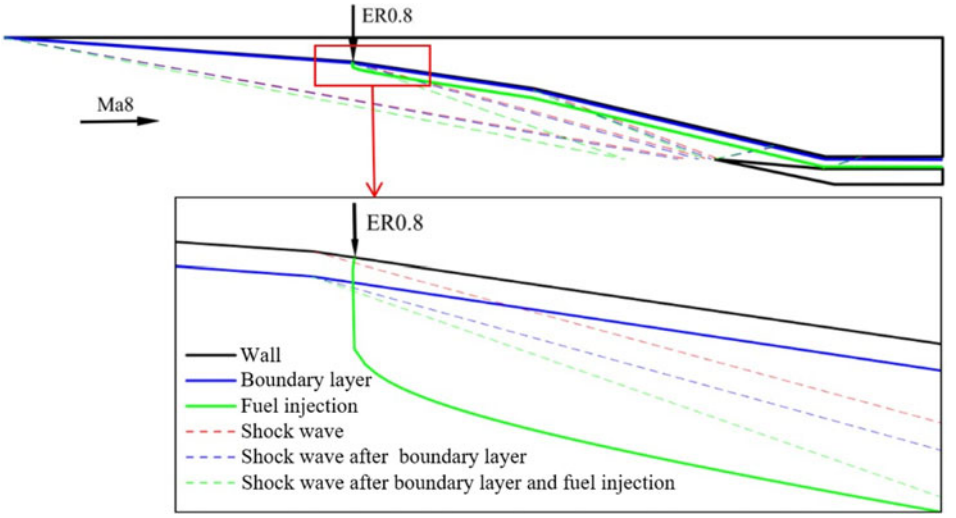


Figure 16. *Schematic diagram of shock wave configuration with fuel injection.*

From the above analysis, it can be seen that the CR and total deflection angle have similar effects on the inlet performance, namely increasing the total pressure recovery coefficient and reducing the cyclic static pressure ratio. And the two parameters show opposite trends of change. In the inlet design, the emphasis is often placed on the total pressure recovery coefficient. The higher the total pressure recovery coefficient, the better the performance, but it is not advisable to solely pursue a high total pressure recovery coefficient. Excessively high total pressure recovery coefficient generally leads to a low cyclic static pressure ratio and static temperature ratio, which can cause a decrease in combustion efficiency in the combustion chamber. Therefore, when designing the inlet, it is necessary to balance and select the appropriate CR and total deflection angle. This paper compromises by selecting the CR of 10 and the total deflection angle of 12.8. All subsequent model analyses are based on the design parameters.

4.2 Effects of fuel pre-injection and heat release

4.2.1 Effects of fuel pre-injection

Under the condition of inflow Mach 8, liquid hydrogen fuel is injected into the inlet with injection vector angle 98° (perpendicular to x axis), the shock wave configuration is shown in Fig. 16. According to the local magnification of the fuel injection diagram, it can be seen that after introducing the boundary layer and fuel injection factors successively, the external oblique shock wave near the injection position is gradually lifted. The diagram visually depicts the effects of the boundary layer and fuel injection on the shock waves, further increasing the compression of inflow.

To specifically understand the effect of fuel injection on inlet performance, the model analysis in the cold state is conducted by using fuel injection with injection vector angle 98° (perpendicular to x axis) at $x = 1.45$m as an example, and the inlet performance parameters are obtained as shown in Fig. 17. Under the same inflow Mach number, as ER of the fuel increases, the flow coefficient gradually decreases, which may be due to the effect of fuel ER on shock wave angle. Under the inflow Mach 12, the flow coefficient of the inlet with fuel injection is 1, indicating that the fuel injection is not strong enough to lift the shock wave out of the cowl lip. By comparing with no fuel injection condition, it is found that the fuel injection increases the total pressure loss and reduces the throat Mach number. Due to the increased shock wave angle after injection, the static pressure in each region increases, leading to an increase in pressure drag. However, the analysis model in this paper does not consider the wall friction, so it shows that the inlet drag coefficient increases after fuel injection.

https://doi.org/10.1017/aer.2025.14 Published online by Cambridge University Press

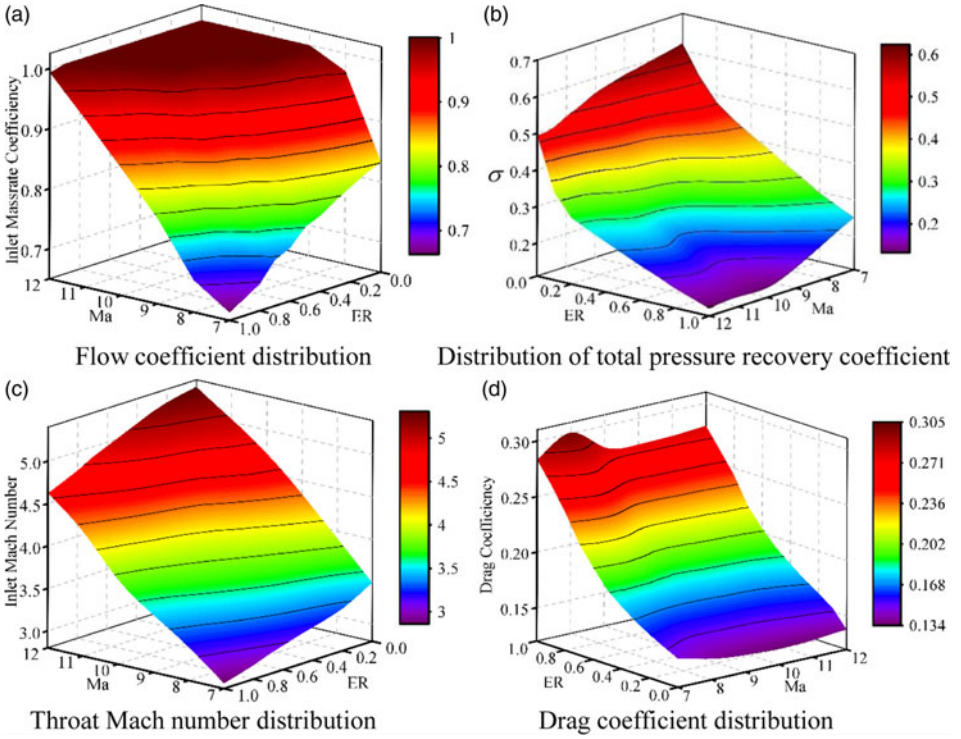


Figure 17. *Variation trend of inlet performance under no-reaction injection conditions.*

4.2.2 Effects of fuel pre-injection and heat release

Based on the results of fuel injection in the cold state, the factor of fuel heat release is added. The performance parameter of the inlet under the hot state is obtained, as shown in Fig. 18. It can be seen that the variation trend of inlet performance parameters with fuel ER and Mach number in the hot state is basically the same as the cold state. As the fuel ER increases, the combustion heat release becomes more pronounced. For a better understanding of the impact of combustion heat release on the performance, the ER 0.2 and 0.4 are chosen for comparison of performance parameters in both cold and hot state, as shown in Fig. 19. In the analysis model of this study, the effect of fuel combustion heat release on the oblique shock angle is not considered, so the flow coefficient remains unchanged. From Fig. 19(b) to (f), it can be observed that considering fuel combustion heat release, the throat Mach number and total pressure recovery coefficient decrease, while the cycle static pressure ratio and cycle static temperature ratio increase. It indicates that injecting fuel into the inlet has the potential to improve thermodynamic cycle efficiency. Overall, fuel injection is equivalent to increasing the compression angle, and the larger the fuel ER, the larger the equivalent compression angle. Based on this understanding, fuel injection can be used to regulate the shock wave position and accurately control the flow rate.

4.3 Comparative analysis of modelling and numerical simulation

The section presents the comparative analysis of modelling and numerical simulation. Among them, the computation time is worthy of attention. The calculation time of the model is a few minutes, which is much less than the computational fluid dynamics (CFD) calculation time. In addition, CFD calculation also needs to draw the grid, and the grid needs to be redrawn every time when the geometry is changed. Therefore, model calculation can save a lot of calculation time compared with CFD calculation. And a further comparison of calculation accuracy is carried out as follows.

https://doi.org/10.1017/aer.2025.14 Published online by Cambridge University Press

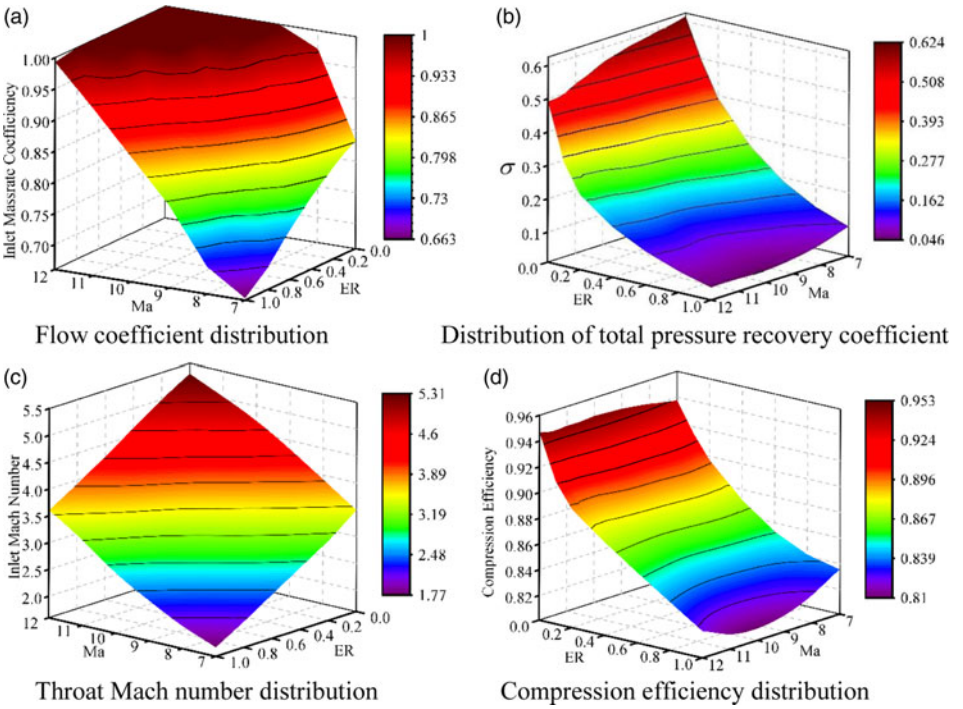


Figure 18. *Variation trend of inlet performance under reaction injection conditions.*

4.3.1 No fuel injection condition

Before the validation of pre-injection model, a comparison between baseline inlet modelling and numerical simulation is conducted, as shown in Fig. 20. Overall, the results of the analysis model have the same variation trend of the performance as the numerical simulation, which basically reflects the performance characteristics of high Mach number inlet during the different inflow conditions. However, the estimation of flow coefficient, total pressure recovery coefficient and throat Mach number is relatively high, probably because the analysis model does not consider the mutual interference between the shock wave and the boundary layer, as well as the reflection of the shock wave. In terms of the drag coefficient, the analytical model and numerical simulation also shows a similar trend, but due to the lack of consideration of factors such as wall friction, the inlet drag coefficient obtained using the analytical model is lower than numerical simulation. In addition, the results obtained by considering the boundary layer factor in the analytical model are closer to numerical simulation results, indicating that the calculation model of the boundary layer in the study is reliable.

4.3.2 Fuel injection condition

A comparison between the analysis model and numerical simulation is conducted under the fuel ER 0.1, 0.2 and 0.4. The injection position for all working conditions is $x = 1.45$m, and the injection vector angle is 98° (perpendicular to x axis). From the Fig. 21, it can be seen the variation trend of shock wave position under the different injection ER is basically consistent between the analytical model and numerical simulation, which implies that the proposed fuel pre-injection and heat release model in the study is reasonable. Furthermore, Figure 22 shows the changes of inlet performance under different injection conditions. In terms of flow coefficient, the analytical model did not consider the effect of bow shock wave at the cowl lip, resulting in a smaller calculation of shock angle. Therefore, the obtained flow coefficient is higher than numerical simulation. In terms of other performance parameters, the analysis

https://doi.org/10.1017/aer.2025.14 Published online by Cambridge University Press

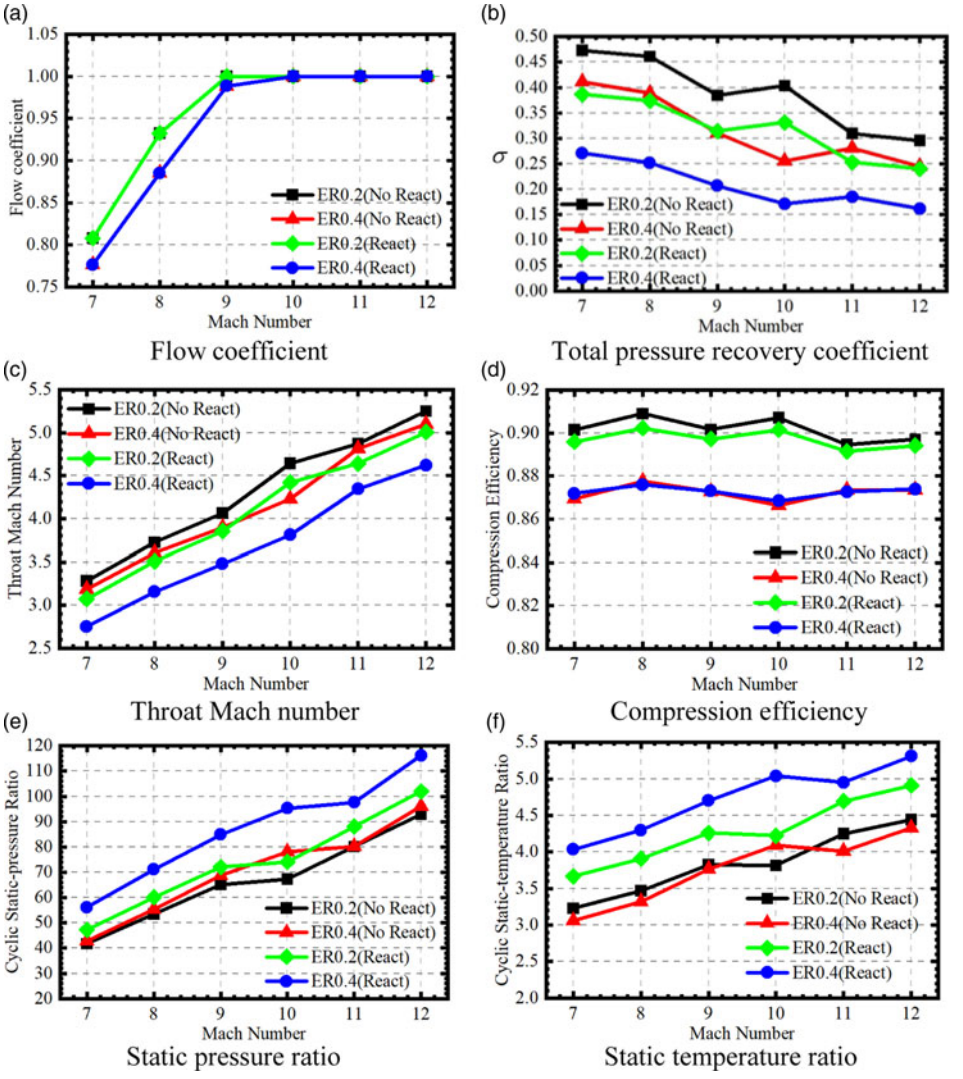


Figure 19. *Performance comparison under reaction and no-reaction injection conditions.*

model accurately estimates the total pressure recovery, throat Mach number, cyclic static temperature ratio and cyclic static pressure ratio, and can reasonably predict the performance changes under the fuel pre-injection conditions. However, the calculation of drag coefficient in the model analysis has a large deviation compared to numerical simulation, which is probably due to the lack of consideration of friction drag and the interaction between the shock wave and boundary layer [38,39]. As described in the reference [38], at high Mach numbers, the friction force accounts for about 20% of the total drag, which is close to the deviation in Fig. 22(d). In the future, the wall friction and the coupling effect of shock wave and boundary layer will be considered in the model to further improve the model accuracy.

5.0 Conclusions

This paper conduct performance modelling of the hypersonic inlet with pre-injection on the basis of the baseline inlet modelling method. And the main conclusions are as follows.

https://doi.org/10.1017/aer.2025.14 Published online by Cambridge University Press

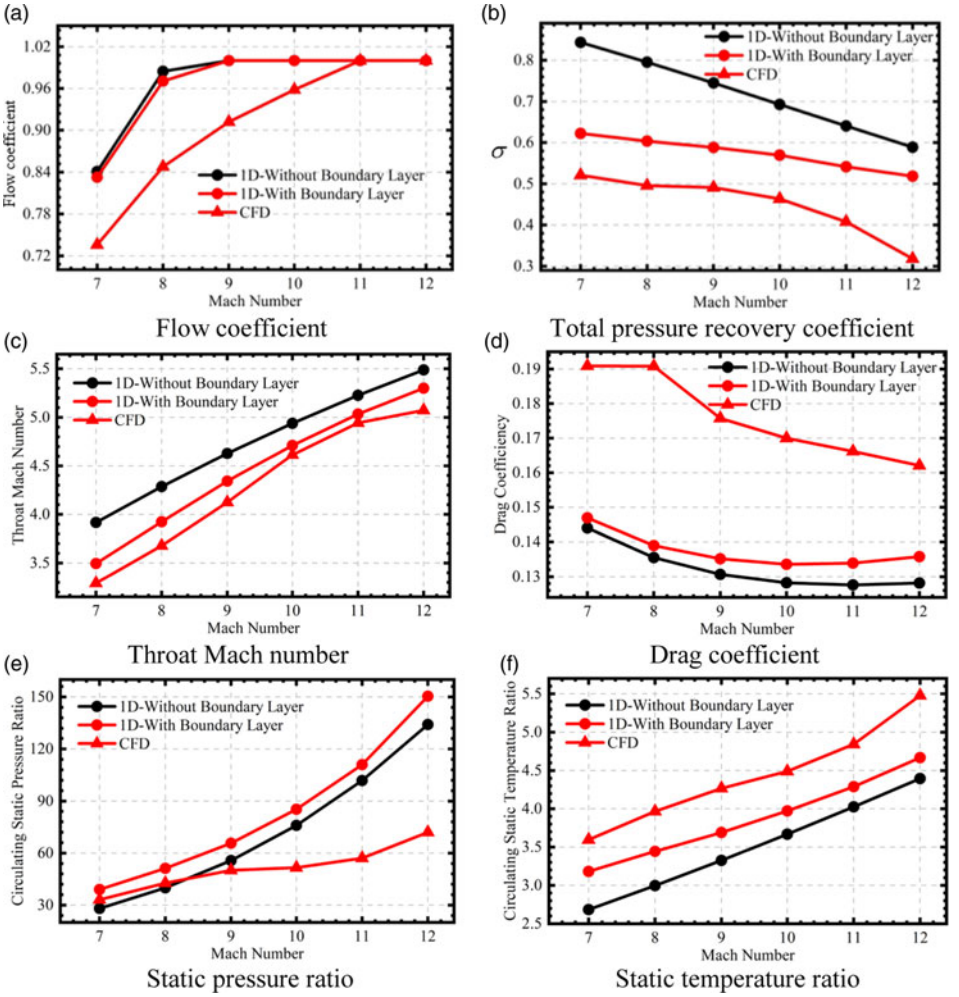


Figure 20. *Comparison of performance parameters between model analysis and numerical simulation.*

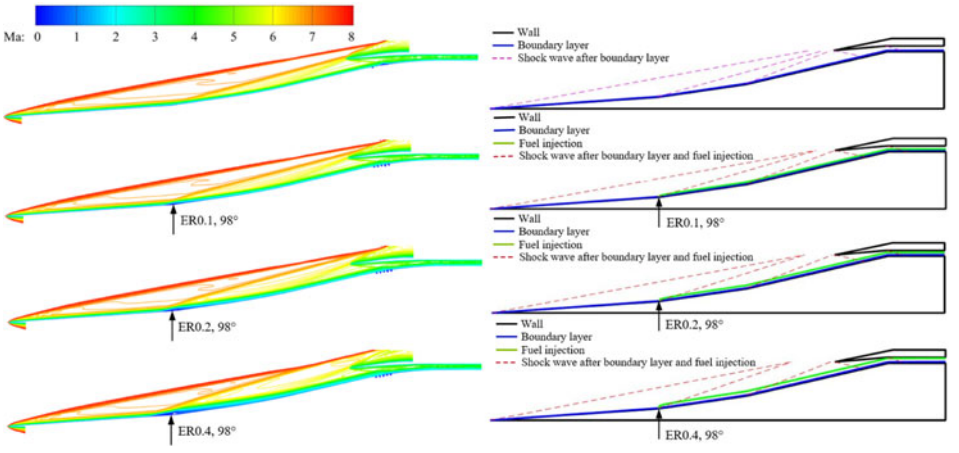


Figure 21. *Comparison of shock waves between analysis model and numerical simulation.*

https://doi.org/10.1017/aer.2025.14 Published online by Cambridge University Press

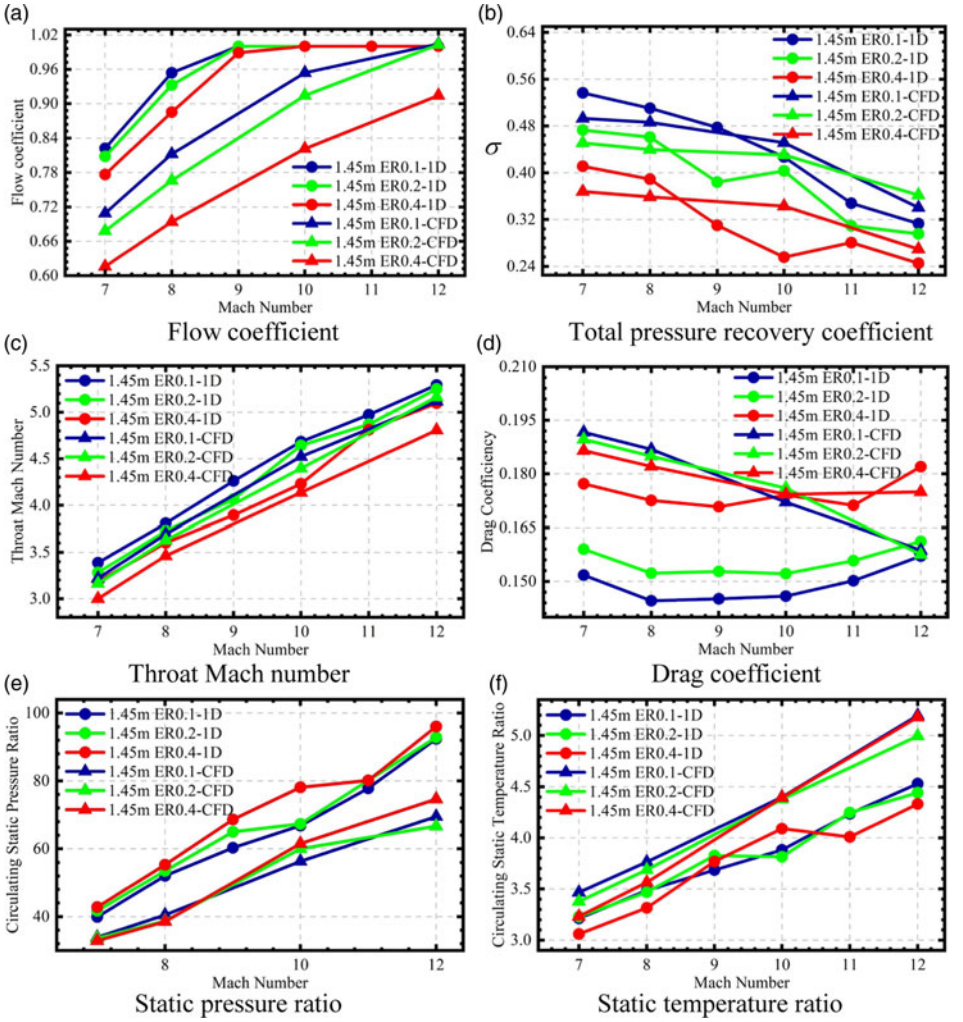


Figure 22. *Comparison of performance parameters between analysis model and numerical simulation.*

In view of the immature equivalent model of fuel pre-injection in the inlet, this paper proposes an inlet pre-injection model. The effect of fuel pre-injection on the performance of the inlet can be divided into cold and hot state. In the cold state, the analysis model equates the effect of fuel injection on the performance of the inlet to an increased compression angle. And in the hot state, the effect of the fuel heat release will be considered in addition to the effect of cold state.

Based on the pre-injection model, the whole inlet performance analysis model considering the effect of fuel pre-injection is established. Then the inlet pre-injection analysis model is validated by using the numerical simulation method. The results show that the analysis model can almost reasonably predict the performance changes under pre-injection conditions. However, the calculation of drag coefficient has some deviation compared to numerical simulation, which is probably due to the lack of consideration of frictional drag and the interaction between the shock wave and boundary layer. In the future the accuracy of the inlet pre-injection model will be further improved by improving the insufficient sub-models and adding some non-critical models.

Acknowledgements. The research effort is supported by the Stable Support Project Funding from National Key Laboratory of Ramjet Technology, Beijing Power Machinery Research Institute.

https://doi.org/10.1017/aer.2025.14 Published online by Cambridge University Press

References

[1] Seleznev, R.K. History of scramjet propulsion development, *J Phys Conf Ser*, 2018, **1009**, (1), pp 1–13.

[2] Das, N., Pandey, K.M. and Sharma, K.K. A brief review on the recent advancement in the field of jet engine-scramjet engine, *Mater Today: Proc*, 2021, **45**, pp 6857–6863.

[3] Cecere, D., Ingenito, A., Giacomazzi, E., Romagnosi, L. and Bruno, C. Hydrogen/air supersonic combustion for future hypersonic vehicles, *Int J Hydrogen Energy*, 2011, **36**, (18), pp 11969–11984.

[4] Capra, B.R., Boyce, R.R., Kuhn M. and Hald, H. Combustion enhancement in a scramjet engine using oxygen enrichment and porous fuel injection, *J Fluid Mech*, 2015, **767**, pp 173–198.

[5] Li, L., Huang, W., Yan, L., Zhao, Z.T. and Liao, L. Mixing enhancement and penetration improvement induced by pulsed gaseous jet and a vortex generator in supersonic flows, *Int J Hydrogen Energy*, 2017, **42**, (30), pp 19318–19330.

[6] Huang, W. Mixing enhancement strategies and their mechanisms in supersonic flows: a brief review, *Acta Astronaut*, 2018, **145**, pp 492–500.

[7] Dharavath, M., Manna, P. and Chakraborty, D. Numerical exploration of mixing and combustion in ethylene fueled scramjet combustor, *Acta Astronaut*, 2015, **117**, pp 305–318.

[8] Vinogradov, V.A., Makarov, A.Y., Potekhina, I.V. and Stepanov, V.V. Numerical and experimental study of fuel pre-injection in the inlet of a high-velocity air-breathing engine, Combustion, *Explos Shock Waves*, 2017, **53**, pp 526–537.

[9] Zhu, C.X., Qiu, R.F., Chen, R.Q. and You, Y.C. Numerical investigation of fuel pre-injection with different injector configurations in hypersonic inlet, *21st AIAA International Space Planes and Hypersonic Technologies Conference*, Xiamen, Fujian, China, 2017.

[10] Guoskov, O.V., Kopchenov, V.I., Lomkov, K.E. and Vinogradov, V.A. Numerical research of gaseous fuel pre-injection in hypersonic three-dimensional inlet, *J Propul Power*, 2001, **17**, (6), pp 1162–1169.

[11] Kim, J.W. and Kwon, O.J. *Numerical simulation of mixing in an inlet-fueled hypersonic-air-breathing propulsion*, ICAS, Daejeon, South Korea, 2016.

[12] Zhu, C.X., Huang, Y.R., Chen, R.Q. and You, Y.C. Study on pre-injection of pyrolysis hydrocarbon fuel in hypersonic inlets, *Propuls Technol*, 2018, **39**, (1), pp 196–202 (in Chinese).

[13] Gardner, A.D., Paull, A. and McIntyre, T.J. Upstream port-hole injection in a 2-D scramjet model, *Shock Waves*, 2002, **11**, pp 369–375.

[14] Turner, J.C. and Smart, M.K. Application of inlet injection to a three-dimensional scramjet at Mach 8, *AIAA J*, 2010, **48**, (4), pp 829–838.

[15] Turner, J.C. and Smart, M.K. Application of radical farming to a 3-D scramjet at Mach 8, *46th AIAA Aerospace Sciences Meeting and Exhibit*, Reno, Nevada, 2008.

[16] Wang, Y.W. and Sislian, J.P. Numerical simulation of gaseous hydrocarbon fuel injection in a hypersonic inlet, *J Propul Power*, 2010, **26**, (5), pp 1114–1124.

[17] Barth, J.E., Wheatley, V. and Smart, M.K. Effects of hydrogen fuel injection in a Mach 12 scramjet inlet, *AIAA Journal*, 2015, **53**, (10), pp 2907–2919.

[18] Barth, J.E., Wheatley, V. and Smart, M.K. Inlet Fuel Injection in a Mach 12 Shape-Transitioning Scramjet, *52nd Aerospace Sciences Meeting, National Harbor*, Maryland, USA, 2014.

[19] Dalle, D.J., Fotia, M.L. and Driscoll, J.F. Reduced-order modeling of two-dimensional supersonic flows with applications to scramjet inlets, *J Propul Power*, 2010, **26**, (3), pp 545–555.

[20] Dalle, D.J., Torrez, S.M. and Driscoll, J.F. Performance analysis of variable-geometry scramjet inlets using a low-order model, *47th AIAA/ASME/SAE/ASEE joint propulsion conference & exhibit*, San Diego, California, USA, 2011.

[21] Zhang, D., Cheng, F., Tang, S., Gong, C.L. and Xu, B. Research on quasi-one-dimensional modeling and performance analysis of RBCC propulsion system, *Int J Turbo Jet-Eng*, 2021, **40**, (3), pp 1–15.

[22] Huo, C., Yang, Z.H., Zhang, Z.Z. and Liu, P.L. Numerical analysis on the conceptual design of an air-breathing engine inlet working in Mach number 3∼5.5, *Proc Inst Mech Eng G J Aerosp Eng*, 2022, **236**, (2), pp 294–307.

[23] Burcat, A. and Ruscic, B. *Third Millenium Ideal Gas and Condensed Phase Thermochemical Database for Combustion with Update from Active Thermochemical Tables*, Argonne National Laboratory, Argonne, IL, 2005.

[24] Stratford, B.S. and Beavers, G.S. *The Calculation of the Compressible Turbulent Boundary Layer in An Arbitrary Pressure Gradient – A Correlation of Certain Previous Methods, Reports and Memoranda No. 3207*, Ministry of Aviation, Aeronautical Research Council, London, 1959.

[25] Xu, X., Chen, B. and Xu, D.J. *Principle and Technology of Ramjet Engine*, Beijing University of Aeronautics and Astronautics Press, 2014 (in Chinese).

[26] Lee, J., Lin, K.C. and Eklund, D. Challenges in fuel injection for high-speed propulsion systems, *AIAA Journal*, 2015, **53**, (6), pp 1405–1423.

[27] Brahmachary, S., Fujio, C. and Ogawa, H. Multi-point design optimization of a high-performance intake for scramjet-powered ascent flight, *Aerosp Sci Technol*, 2020, **107**, pp 106362.

[28] Segal, C. *The Scramjet Engine: Processes and Characteristics*, Cambridge, England, 2009.

[29] Birzer, C.H. and Doolan, C.J. Quasi-one-dimensional model of hydrogen-fueled scramjet combustors, *J Propul Power*, 2009, **25**, (6), pp 1220–1225.

[30] Gerlinger, P. and Bruggemann, D. Numerical investigation of hydrogen strut injections into supersonic airflows, *J Propul Power*, 2000, **16**, (1), pp. 22–28.

[31] Curran, E.T., Murthy, S.N.B. *Scramjet Propulsion*, Progress in Astronautics and Aeronautics, AIAA, Washington, DC, 2001.

[32] Gerdroodbary, M.B. *Scramjets: Fuel Mixing and Injection Systems*, Butterworth-Heinemann, England, 2020.

https://doi.org/10.1017/aer.2025.14 Published online by Cambridge University Press

[33] Li, N., Chang, J.T., Tang, J.F., Yu, D.R., Bao, W. and Song, Y.P. Effect of control route on the unstart/restart characteristics of an over-under TBCC inlet, *Adv Aircr Spacecr Sci*, 2018, **5**, (4), pp 431–444.
[34] Shi, W., Chang, J.T., Zhang, J.L., Wang, Y.Y., Hou, W.X. and Bao, W. Numerical investigation on behaviors of shock train in a hypersonic inlet with translating cowl, *Acta Astronaut*, 2018, **152**, pp 682–691.
[35] Ding, F., Shen, C.B., Huang, W. and Liu, J. Numerical validation and back-pressure effect on internal compression flows of typical supersonic inlet. *Aeronaut J*, 2015, **119**, (1215), pp 631–645.
[36] Ye, J., Zhang, Z., Dai, M., Nie, S., Qin, F. and Wei, X.G. Combustion organization strategies for a variable geometry RBCC combustor under low total temperature conditions, *Appl Therm Eng*, 2024, **236**, p 121782.
[37] Odam, J. and Paull, A. Internal combustor scramjet pressure measurements in the T4 shock tunnel, *AIAA Joint Space Planes and Hypersonic Systems and Technology Conference*, Orleans, France, 2002.
[38] Wei, Y.B., Zhang, K.Y. and Luo, X.C. Analysis and research on internal resistance characteristics of two-dimensional hypersonic inlet, *Acta Aerodyn Sinica*, 2010, **28**, (1), 104–108 (in Chinese).
[39] Gopal, V. and Wilson, D. Reduced-order analysis of scramjet inlet operation, *54th AIAA Aerospace Sciences Meeting*, California, USA, 2016.

Cite this article: Luo F.T., Li H.T., Qu Z.M., Chen W.J. and Long Y.S. (2025). Performance modelling and numerical simulation validation of hypersonic inlet with fuel pre-injection. *The Aeronautical Journal*, **129**, 2283–2306. https://doi.org/10.1017/aer.2025.14

https://doi.org/10.1017/aer.2025.14 Published online by Cambridge University Press